Increased brain tissue sodium concentration in Friedreich ataxia: A multimodal MR imaging study

Janna Krahe [a,b], Imis Dogan [a,b], Claire Didszun [a], Shahram Mirzazade [a], Alexa Haeger [a,b], Nadim Joni Shah [a,b,c,d], Ilaria A. Giordano [e,f], Thomas Klockgether [e,f], Guillaume Madelin [g], Jörg B. Schulz [a,b], Sandro Romanzetti [a,b,1], Kathrin Reetz [a,b,1,*]

[a] *Department of Neurology, RWTH Aachen University, Pauwelsstr. 30, 52074 Aachen, Germany*
[b] *JARA-BRAIN Institute Molecular Neuroscience and Neuroimaging, Research Centre Juelich GmbH and RWTH Aachen University, 52074 Aachen, Germany*
[c] *Institute of Neuroscience and Medicine 4 (INM-4), Research Centre Juelich GmbH, 52428 Juelich, Germany*
[d] *Monash Institute of Medical Engineering, Department of Electrical and Computer Systems Engineering, and Monash Biomedical Imaging, School of Psychological Sciences, Monash University, Melbourne, VIC 3800, Australia*
[e] *Department of Neurology, University Hospital of Bonn, Venusberg-Campus 1, 53127 Bonn, Germany*
[f] *German Center for Neurodegenerative Diseases (DZNE), Venusberg-Campus 1, 53127 Bonn, Germany*
[g] *Center for Biomedical Imaging, Department of Radiology, New York University Grossman School of Medicine, New York NY10016, USA*

A R T I C L E I N F O

A B S T R A C T

In patients with Friedreich ataxia, structural MRI is typically used to detect abnormalities primarily in the brainstem, cerebellum, and spinal cord. The aim of the present study was to additionally investigate possible metabolic changes in Friedreich ataxia using *in vivo* sodium MRI that may precede macroanatomical alterations, and to explore potential associations with clinical parameters of disease progression.

Tissue sodium concentration across the whole brain was estimated from sodium MRI maps acquired at 3 T and compared between 24 patients with Friedreich ataxia (21–57 years old, 13 females) and 23 controls (21–60 years old, 12 females). Tensor-based morphometry was used to assess volumetric changes. Total sodium concentrations and volumetric data in brainstem and cerebellum were correlated with clinical parameters, such as severity of ataxia, activity of daily living and disability stage, age, age at onset, and disease duration.

Compared to controls, patients showed reduced brain volume in the right cerebellar lobules I-V (*difference in means*: −0.039% of total intracranial volume [TICV]; Cohen's $d = 0.83$), cerebellar white matter (WM) (-0.105% TICV; $d = 1.16$), and brainstem (-0.167%TICV; $d = 1.22$), including pons (-0.102%TICV; $d = 1.00$), medulla (-0.036%TICV; $d = 1.72$), and midbrain (-0.028%TICV; $d = 1.05$). Increased sodium concentration was additionally detected in the total cerebellum (*difference in means*: 2.865 mmol; $d = 0.68$), and in several subregions with highest effect sizes in left (5.284 mmol; $d = 1.01$) and right cerebellar lobules I-V (5.456 mmol; $d = 1.00$), followed by increases in the vermis (4.261 mmol; $d = 0.72$), and in left (2.988 mmol; $d = 0.67$) and right lobules VI-VII (2.816 mmol; $d = 0.68$). In addition, sodium increases were also detected in all brainstem areas (3.807 mmol; $d = 0.71$ to 5.42 mmol; $d = 1.19$). After controlling for age, elevated total sodium concentrations in right cerebellar lobules IV were associated with younger age at onset ($r = -0.43$) and accordingly with longer disease duration in patients ($r = 0.43$).

Our findings support the potential of *in vivo* sodium MRI to detect metabolic changes of increased total sodium concentration in the cerebellum and brainstem, the key regions in Friedreich ataxia. In addition to structural changes, sodium changes were present in cerebellar hemispheres and vermis without concomitant significant atrophy. Given the association with age at disease onset or disease duration, metabolic changes should be further investigated longitudinally and in larger cohorts of early disease stages to determine the usefulness of sodium MRI as a biomarker for early neuropathological changes in Friedreich ataxia and efficacy measure for future clinical trials.

1. Introduction

Friedreich ataxia is the most common autosomal-recessively inherited neurodegenerative ataxia, mainly caused by a guanosine-adenosine-adenosine (GAA) trinucleotide repeat expansion in the FXN gene encoding the protein frataxin, (Campuzano et al., 1996) in which the mitochondrial energy production is disturbed. Aside from the major symptom ataxia, Friedreich ataxia is a chronic complex and multisystem neurodegenerative disease with various symptoms such as coordination problems, poor balance, dysarthria, weakness, ocular fixation instability, deep sensory loss, and visual and hearing impairment, (Harding, 1981) as well as non-neurological manifestations such as hypertrophic cardiomyopathy, (Hewer, 1968) diabetes mellitus, (Thorén, 1962) kyphoscoliosis, and foot deformities (Reetz et al., 2018). Disease onset mostly occurs around puberty (typical onset) and in fewer cases later in life (late onset) (Harding, 1981; Friedreich, 1863).

The natural history study European Friedreich Ataxia Consortium for Translational Studies (EFACTS; https://www.e-facts.eu) investigates progression characteristics and clinical outcome measures, providing recommendations for the design of upcoming clinical trials in Friedreich ataxia (Reetz et al., 2015; Reetz et al., 2016; Reetz et al., 2021). Given the slowly progressive nature of the disease, predictors of faster disease progression, such as an early age of onset, (Harding, 1981; Reetz et al., 2015; Metz et al., 2013). are becoming increasingly important in Friedreich ataxia research, accompanied by the search for alternative and potentially more sensitive imaging markers to monitor disease progression and to be used in clinical trials.

Magnetic resonance imaging (MRI) has been used to detect primarily structural abnormalities in the brainstem, cerebellum, and spinal cord, whereas changes in cerebral regions are less pronounced in Friedreich ataxia (França et al., 2009; Dogan et al., 2016; Dogan et al., 2018; Koeppen and Mazurkiewicz, 2013). It is of upmost interest, however, to detect pathological changes as early as possible, potentially prior to overt and irreversible structural neurodegeneration as observed by conventional MRI (Reetz et al., 2019). Sodium (^{23}Na) plays an important role in many cellular functions, such as cellular homeostasis and electrochemical signaling pathways. In healthy tissue, there is a large sodium concentration gradient between intracellular (10–15 mmol) and extracellular areas (140–150 mmol), regulated by the sodium–potassium pump (Na^+/K^+-ATPase) across the cell membrane. Cellular impairment, mitochondrial dysfunction or other disturbances of Na^+/K^+-ATPase lead to an increase in intracellular sodium concentration (Madelin and Regatte, 2013). Sodium dysbalances, in turn, could thus indicate early cellular dysfunction before degeneration of the cell (Boada et al., 2005). Therefore, sodium MRI can be used to detect metabolic changes that may even precede structural changes in neurodegenerative diseases by measuring the total tissue sodium concentration (TSC). TSC is assessed by the volume-fraction-weighted mean of the intracellular sodium concentration and the extracellular sodium concentration (Christensen et al., 1996). Increased sodium concentration has been shown in patients due to tumorous, (Hashimoto et al., 1991; Ouwerkerk et al., 2003; Thulborn et al., 2009; Nagel et al., 2011) and stroke conditions, (Thulborn et al., 1999; Hussain et al., 2009; Inglese et al., 2010; Boada et al., 2012) and also in demyelinating or neurodegenerative pathologies such as multiple sclerosis, (Inglese et al., 2010; Zaaraoui et al., 2012; Petracca et al., 2016) or Alzheimer's disease

(Mellon et al., 2009). We also presented first results in Huntington's disease towards an increase in sodium concentration in the bilateral striatum, a key region in this disease (Reetz et al., 2012). Recently, we showed increased sodium concentrations in Alzheimer's disease with sodium MRI at 7 Tesla, (Haeger et al., 2021) and are currently evaluating sodium concentration as an outcome measure in a multicomponent exercise intervention in Alzheimer's pathology (Haeger et al., 2020).

In Friedreich ataxia in particular, the metabolic approach is of major interest because of the underlying genetic basis of mutations in the gene encoding the mitochondrial protein frataxin. Studies using ^{31}P magnetic resonance spectroscopy (MRS) in heart and muscle areas suggest mitochondrial dysfunction and impaired energy metabolism in Friedreich ataxia (Vorgerd et al., 2000; Hart et al., 2005; Lodi et al., 1999). In the current study, we used metabolic and structural MRI to investigate: a) sodium concentration and volume differences in the brain of patients with Friedreich ataxia compared to controls, and b) to explore potential associations between TSC levels, brain volume, and clinical parameters. This first ^{23}Na-MRI study in Friedreich ataxia may provide us with first insights into metabolic changes as well as the potential of TSC measurement as an imaging marker for Friedreich ataxia.

2. Materials and methods

2.1. Participants

Adult patients with genetically confirmed Friedreich ataxia without other neurological conditions and MRI contraindication were eligible for this study and were recruited within the framework of EFACTS at the Department of Neurology of the RWTH Aachen University Hospital. Initially, 24 patients and 24 age- and sex-matched healthy controls without history of neurological or psychiatric disorders were included. However, data of one control participant had to be excluded due to technical issues, resulting in 23 healthy controls and 24 patients in the final analysis. Most patients had typical age of onset (21 patients with age of onset ≤ 24 years) and homozygous GAA repeat expansions ($N = 23$), and only three patients with late age of onset (≥25 years).[7] One patient was compound heterozygote with a point mutation of start codon ATG. Age (t [45] = -0.12, $p = 0.904$) and sex (x2 [1] = 0.02, $p = 0.891$) did not differ between both groups. Detailed sample characteristics and demographics are provided in Table 1.

Ethical approval (EK 083/15) was given by the Institutional Review Board of the RWTH Aachen University Hospital, and all participants signed the respective declaration of consent prior to study participation.

2.2. Clinical assessments

Clinically, ataxia was assessed with the Scale for the Assessment and Rating of Ataxia (SARA) (Schmitz-Hubsch et al., 2006). Higher scores on this 40-point scale indicate more severe ataxia. Also, the Activity of Daily Living scale (ADL), as part of the FARS (Friedreich Ataxia Rating Scale), (Subramony et al., 2005) was used in a structured guided interview setting to quantify disease severity by assessing daily functional activity impairment (maximal severity-score 36). Furthermore, disease stage was rated based on the SDFS (spinocerebellar degeneration functional score) (Anheim et al., 2009) ranging from 0 (no functional

Table 1
Demographic and clinical characteristics of the total sample.

	Patients with Friedreich ataxia	Controls
Demographics		
N (%)	24 (100 %)	23 (100 %)
Female/Male (%)	13 (54%) / 11 (46%)	12 (52%) / 11 (48%)
Age (years)	35.58 ± 11.07	35.17± 12.04
Disease onset		
Age of onset (years)	16.29 ± 6.82	–
Typical onset (%)	21 (88 %)	–
Late onset (%)	3 (12 %)	–
Disease duration (years)	19.29 ± 9.23	–
Genetics		
GAA repeats:		
Allele 1	518.50 ± 217.08	33.71 ± 13.89
Allele 2	805.79 ± 194.83	33.71 ± 13.89
Point mutation (%)	1 (4 %)[a]	0
Disease severity		
SARA score	17.79 ± 9.12	0.03 ± 0.12
ADL score	13.13 ± 6.87	0.17 ± 0.71
Disability stage	4.58 ± 1.25	0
Ambulatory (%)	17 (71 %)	23 (100%)
Non-ambulatory (%)	7 (29 %)	0

Data are presented as mean ± standard deviation or n (%) ; N = sample size; typical onset = age at onset ≤ 24 years; late onset = age at onset ≥ 25 years; GAA1 / GAA2 = GAA-repeat length on allele 1 / allele 2: data are missing for 7 controls; apoint mutation = mutation of start codon ATG; SARA = Scale for the assessment and rating of ataxia (maximal severity-score 40): data are missing for 6 controls; ADL = Activity of daily living scale (maximal severity-score 36): data are missing for 6 controls; disability stage = spinocerebellar degeneration functional score (SDFS; maximal severity-score 7); ambulatory = SDFS 1 – 5 (no functional handicap but signs at examination – walking with two sticks); non-ambulatory = SDFS 6 – 7 (unable to walk, requiring wheelchair – confined to bed).

handicap) to 6 (unable to walk, requiring wheelchair), and 7 (confined to the bed). All clinical assessments were performed in the facilities of the Department of Neurology, RWTH Aachen University Hospital, Germany.

2.3. MRI acquisition

All MRI scans were performed on a 3 Tesla whole-body MR scanner (PRISMA Software version VD13D, Siemens Medical Systems, Erlangen). Anatomical T1-weighted images of the head were acquired using a MPRAGE (Magnetization Prepared Rapid-Acquisition Gradient Echo) sequence performed with a 64-channel head-neck proton (^{1}H) coil: TR (repetition time) = 2300 ms, TI (inversion time) = 900 ms, TE (echo time) = 2.3 ms, FA (flip angle) = 7°, TA (acquisition time) = 7 min, at 0.8 mm isotropic resolution.

For sodium measurements, we used a variable-flip-angle (VFA) technique as described previously by our group (Coste et al., 2019). This technique is based on two ultra-short echo time sodium images acquired with the FLORET (fermat looped, orthogonally encoded trajectories) (Pipe et al., 2011) sequence in the spoiled steady-state at two optimal FA (TR = 20 ms, TE = 0.475 ms, hubs α_1/α_2 = 25°/55°, interleaves = 100, hubs = 3, hub angle = 45°, readout duration = 10 ms). A dual-resonance ^{1}H/^{23}Na quadrature birdcage coil (Rapid Biomed GmbH, Rimpar, Germany) was used to perform the sodium measurements. Two cylindrical agarose gel (2% w/w) calibration phantoms of known sodium concentrations (51 and 102 mmol/l) placed on both sides of the head of the participant at about 1.5 cm away from the temporal lobes were used for calibration. Calibration of the sodium 90° RF (radio frequency) pulse was performed manually at the beginning of each session using a series of non-localized pulse-acquire spectra (Coste et al., 2019). The sodium imaging session consisted of a series of short scans, each 3-minutes long. We performed three sodium scans at each FA to improve the final signal-to-noise ratio (SNR) of final images, resulting in a total scan time of 18

min. The resolution of the sodium images was 4 mm isotropic. Two images at FA of 60° and 120° (TE/TR = 0.5/80 ms; 6 mm isotropic resolution) were acquired with the same FLORET sequence after the main sodium measurement session to estimate the coil excitation map. This was later used in our quantification pipeline to correct for residual B1 homogeneity. The (sodium reconstruction) pipeline included a motion correction step, which aligned all images to adjust for involuntary movements of the participants (Coste et al., 2019).

2.4. MRI data processing

2.4.1. Processing of structural MRI data

Each structural scan was preprocessed using the *antsCorticalthickness* pipeline, (Tustison et al., 2014) provided in the Advanced Normalization Tools (ANTs) (Avants et al., 2011), and segmented in subject space into gray matter, white matter, deep gray matter, cerebellum, and brainstem.

In a further step, regions of interest (ROIs) within the cerebellum and brainstem were identified using the spatially unbiased infra-tentorial (SUIT) cerebellar atlas by Diedrichsen (Diedrichsen, 2006). Given the insufficient resolution of sodium imaging for individual cerebellar lobules, for both structural and sodium MRI analyses the cerebellum was subdivided into cerebellar lobules I-V, VI-VII, VIII-X (for each hemisphere, respectively), vermis, and cerebellar white matter (WM). The brainstem was subdivided into pons, medulla, and midbrain.

A minimum deformation template (MDT) was created from all anatomical scans of the control group. During this process, labels for total gray matter, total white matter, deep gray matter, brainstem, and cerebellum in template space, were estimated by means of a joint label fusion procedure (Wang et al., 2013). Successively, each individual stuctural scan of both control and patient groups were normalized to the MDT using a combination of linear and non-linear geometrical transformation (Hua et al., 2008).

2.4.2. Processing of sodium MRI data

Processing of each raw k-space data set corresponding to each short scan was performed offline on a standard desktop computer after downloading the raw data from the scanner. Each raw data set was first filtered with a Hanning filter and successively reconstructed into a complex image using a NUFFT (non-uniform fast Fourier transform) (Fessler and Sutton, 2003) algorithm implemented in MATLAB (The Mathworks, Natick, USA).

The three complex images reconstructed for each FA were individually denoised, mutually aligned using a rigid-body transformation and finally averaged in complex space. The two resulting ^{23}Na images at FA = 25° and FA = 55° were then combined, taking into account any B1-inhomogeneity, according to the VFA method as described in Coste *et al.,* (Coste et al., 2019). The VFA method produced ^{23}Na M_0 (spin-density) images which were corrected for partial volume effects using an iterative Van-Citter approach included in the PET-PVC (partial volume correction) (Thomas et al., 2016) toolbox.

To transform ^{23}Na M_0 images into TSC maps, the mode of the distribution of the signal intensity of both the 2% agarose reference gels was estimated and used to obtain a two-point calibration curve, which has already been used in previous work (Inglese et al., 2010; Reetz et al., 2012; Coste et al., 2019). We used the mode instead of the mean of the signal distributions to take into account the skewedness of the sodium signal distribution. The calibration was then applied to convert the signal in each voxel into TSC values. Finally, individual TSC maps were co-registered to their T1-weighted anatomical reference images with ANTs. For co-registration, T1 images were down-sampled to 4 mm voxel-size and their signal inverted to resemble the contrast of the TSC maps. A rigid co-registration was then performed only on the brain tissue. In Supplementary Fig. 1, examples of ^{1}H data, ^{23}Na images and transformed TSC maps are shown.

2.5. Statistical analysis

2.5.1. Whole-brain analysis of MRI data

To compare volumetric changes between healthy controls and Friedreich ataxia patients, we performed a whole-brain tensor-based morphometry (TBM) analysis. The log-jacobians of the geometrical transformations used to normalize each brain to the MDT were analyzed using a cluster-based permutation approach. This was performed with the BROCCOLI toolbox. A cluster-extent threshold of 2.5 was used to define the minimum cluster size. The permutation analysis resulted in Student's t-test maps, which by the very nature of the permutation test were already corrected for multiple comparisons.

To perform a whole-brain analysis of TSC levels in both groups, we first created a TSC study template using ANTs. All TSC maps from both groups were then projected into this template space in which the final voxel-wise comparison was performed. Similarly to the TBM analysis, a cluster-based permutation analysis was performed with the BROCCOLI toolbox ($p < 0.05$). The resulting t-test map allowed us to identify clusters of differences between groups in the whole brain, including disease-related (cerebellum and brainstem) and non-disease related areas.

2.5.2. ROI-based analysis of cerebellum and brainstem

Average TSC values and volumes extracted from the SUIT ROIs of the cerebellum (cerebellar lobules I-V, VI-VII, VIII-X [for each hemisphere, respectively], vermis, cerebellar WM), and brainstem (pons, medulla, and midbrain) were compared between both groups using two-sample t-tests and Cohen's d as effect size measure with a 0.20 criterion for a small effect, a 0.50 criterion for a medium effect, and a 0.80 criterion for a large effect (Cohen, 1988). Additionally, we performed subgroup analyses comparing typical-onset or ambulatory patients to controls, respectively. All brain volume data (mm^3) were normalized by the total intracranial volume (TICV) to correct for interindividual differences in brain size, and are expressed as percentage (%) of TICV. To correct for multiple comparisons within the cerebellum (eight ROIs) and brainstem (three ROIs) the Benjamini-Hochberg procedure controlling the false discovery rate (FDR) was applied (Benjamini and Hochberg, 1995).

Finally, Pearson's correlation coefficients were calculated between age and MRI data (brain volume and TSC) for both groups, and first-order partial correlations with age as a covariate for the patient group to exploratively investigate associations of TSC values with brain volumes, and clinical parameters. The ROI-based statistical analysis was performed in IBM SPSS 24 statistics with $p < 0.05$ (two-tailed) set as the threshold for statistical significance.

2.6. Data availability

Raw data were generated at the Department of Neurology of the RWTH Aachen University Hospital. Derived data supporting the findings of this study are available from the corresponding author on reasonable request.

3. Results

3.1. Brain volume data

Whole-brain comparisons of brain volume data between patients with Friedreich ataxia and controls revealed a reduction in volume exclusively in the cerebellum and brainstem of patients (Fig. 1, Table 2). Subsequent ROI-based testing in subregions of the cerebellum revealed reduced volumes in Friedreich ataxia patients compared to controls in the right cerebellar lobules I-V (t [45] = 2.85, $p = 0.026$, $d = 0.83$), and in cerebellar WM (t [45] = 3.96, $p = 0.002$, $d = 1.16$), each with a large effect size. Marked differences were also found across the total brainstem with reduced volumes in the patient group (t [45] = 4.19, $p < 0.001$, $d = 1.22$), and in its subregions with the highest effect size for the medulla (t [45] = 5.88, $p < 0.001$, $d = 1.72$), followed by the midbrain (t [45] = 3.60, $p = 0.001$, $d = 1.05$), and the pons (t [45] = 3.44, $p = 0.001$, $d = 1.00$). Other group differences were not significant (Fig. 2A, Table 2).

In a sub-analysis after excluding the three late-onset patients, similar volume differences were found in typical-onset patients ($N = 21$) compared to controls, except that volume changes in the right cerebellar lobules I-V were not significant after correction for multiple testing (Supplementary Table 1).
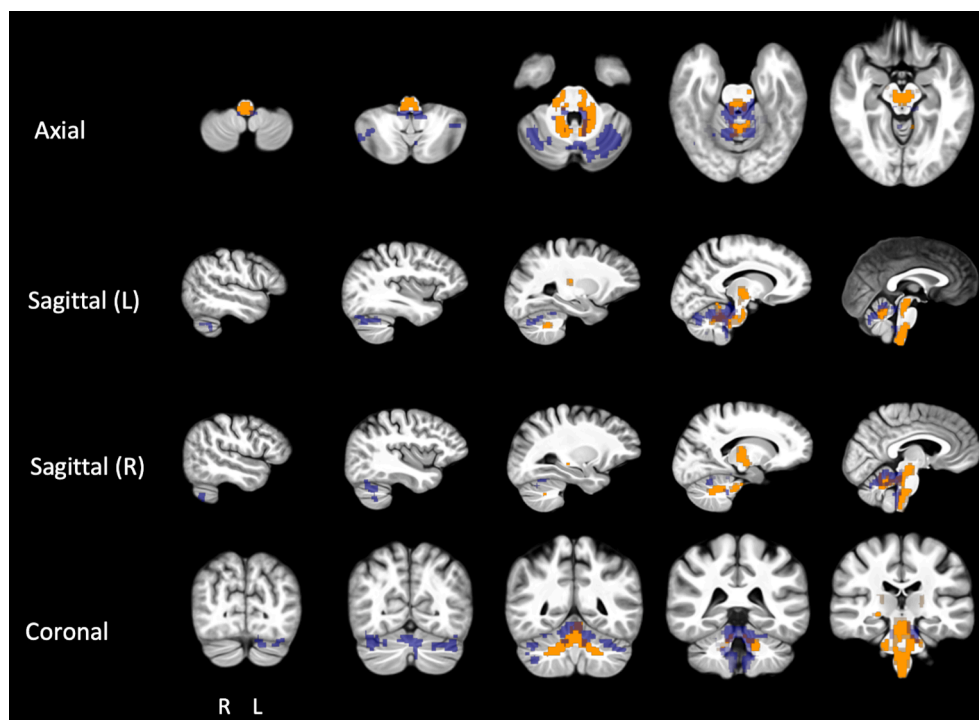
Fig. 1. Visualization of group differences in brain volume (orange) and total sodium concentration (blue) between patients with Friedreich ataxia and controls. Group differences in brain volume (patients < controls, $p < 0.05$; highlighted in *orange*) calculated using tensor-based morphometry. Overlayed group differences in total sodium concentration (patients > controls, $p < 0.05$; highlighted in *blue*) calculated using voxel-based permutation analysis performed with BROCCOLI. Both whole-brain analyses showed significant changes in cerebellum and brainstem. The colors show differences significant at $p < 0.05$. The brain slices shown represent the range between the respective endpoints where the differences of total sodium concentration are still visible. *Abbreviations*: Sagittal (L/R) = left/rigth hemisphere sagittal section. (For interpretation of the references to colour in this figure legend, the reader is referred to the web version of this article.)

Table 2
Brain volume and tissue sodium concentration of cerebellum and brainstem in patients with Friedreich ataxia compared to controls.

Region of interest	Hemis-phere (L / R)	Brain volume (% of TICV)			TSC (mmol/l)		
		Friedreich ataxia Mean ± SD	Controls Mean ± SD	Effect size (d)	Friedreich ataxia Mean ± SD	Controls Mean ± SD	Effect size (d)
Brainstem	L / R	1.606 ± 0.127	1.773 ± 0.145	**1.22***	45.704 ± 5.111	41.566 ± 3.628	**0.93**
Pons	L / R	0.952 ± 0.097	1.054 ± 0.107	**1.00**	44.056 ± 5.143	40.306 ± 3.849	**0.82***
Medulla	L / R	0.299 ± 0.021	0.335 ± 0.021	**1.72***	44.703 ± 6.366	40.896 ± 4.026	**0.71***
Midbrain	L / R	0.356 ± 0.025	0.384 ± 0.029	**1.05**	51.238 ± 4.966	45.818 ± 4.099	**1.19**
Cerebellum	L / R	10.117 ± 0.798	10.182 ± 0.638	0.09	42.511 ± 4.344	39.646 ± 4.074	**0.68***
I-V	L	0.540 ± 0.057	0.573 ± 0.044	0.65+	55.243 ± 5.166	49.959 ± 5.278	**1.01**
	R	0.572 ± 0.057	0.611 ± 0.035	**0.83***	54.720 ± 5.633	49.264 ± 5.230	**1.00**
VI-VII	L	2.752 ± 0.261	2.730 ± 0.215	0.09	40.939 ± 4.369	37.951 ± 4.488	**0.67***
	R	2.734 ± 0.258	2.752 ± 0.183	0.08	40.889 ± 4.310	38.073 ± 3.897	**0.68***
VIII-X	L	1.008 ± 0.092	0.967 ± 0.099	0.44	39.702 ± 4.223	37.610 ± 4.698	0.47
	R	0.995 ± 0.102	0.942 ± 0.099	0.53	38.685 ± 5.247	37.789 ± 4.443	0.18
Vermis	L / R	0.437 ± 0.044	0.424 ± 0.037	0.32	54.382 ± 6.117	50.121 ± 5.696	**0.72***
Cerebellar WM	L / R	1.078 ± 0.101	1.183 ± 0.079	**1.16**	38.965 ± 4.661	36.494 ± 4.158	0.56
Cerebrum							
Frontal lobe	L	13.309 ± 0.387	13.416 ± 0.536	0.23	40.903 ± 4.613	39.623 ± 4.869	0.27
	R	13.183 ± 0.334	13.432 ± 0.622	0.50	41.420 ± 4.611	39.965 ± 4.809	0.31
Temporal lobe	L	4.965 ± 0.210	4.903 ± 0.265	0.26	40.642 ± 4.128	39.815 ± 3.956	0.20
	R	5.090 ± 0.241	5.059 ± 0.189	0.14	40.745 ± 3.973	39.754 ± 3.828	0.25
Parietal lobe	L	5.645 ± 0.278	5.699 ± 0.245	0.21	44.697 ± 4.942	43.158 ± 4.863	0.31
	R	5.791 ± 0.236	5.795 ± 0.214	0.02	44.572 ± 4.352	42.825 ± 4.854	0.38
Occipital lobe	L	2.537 ± 0.286	2.502 ± 0.277	0.12	43.079 ± 4.229	41.451 ± 4.063	0.39
	R	2.312 ± 0.280	2.235 ± 0.237	0.30	43.323 ± 4.268	42.102 ± 4.265	0.29

Data are presented as mean ± standard deviation. Brain volumes are adjusted for total intracranial volume (TICV) and displayed in % (TICV = 100%). Significant group differences between patients with Friedreich ataxia (N = 24) and controls (N = 23) at *$p < 0.05$, **$p < 0.01$ or ***$p < 0.001$ (adjusted for multiple testing using the Benjamini-Hochberg procedure within the brainstem and cerebellar regions, respectively); +not significant after Benjamini-Hochberg procedure. Criteria for the evaluation of effect sizes (Cohen's d): 0.20 = small effect, 0.50 = medium effect, 0.80 = large effect. Abbreviations: L = left; R = right; TSC = total sodium concentration.

3.2. TSC levels

Similar to structural MRI findings, whole-brain analysis did not reveal TSC differences in the cerebrum but TSC increases in patients with Friedreich ataxia in the anterior cerebellum and brainstem (Fig. 1, Table 2). ROI-based analyses of TSC levels showed increases of TSC in patients in the total cerebellum ($t [45] = -2.33$, $p = 0.024$, $d = 0.68$), with most pronounced differences in left ($t [45] = -3.47$, $p = 0.009$, $d = 1.01$) and right cerebellar lobules I-V ($t [45] = -3.44$, $p = 0.005$, $d = 1.00$), followed by changes in the vermis ($t [45] = -2.47$, $p = 0.046$, $d = 0.72$), and in right ($t [45] = -2.35$, $p = 0.047$, $d = 0.68$) and left ($t [45] = -2.31$, $p = 0.041$, $d = 0.67$) cerebellar lobules VI-VII. Here, TSC differences in cerebellar WM did not reach significance between the two groups ($t [45] = -1.92$, $p = 0.062$, $d = 0.56$). Increased TSC was also found in total brainstem ($t [45] = -3.19$, $p = 0.003$, $d = 0.93$), including midbrain with the highest effect size ($t [45] = -4.07$, $p = 0.001$, $d = 1.19$), pons ($t [45] = -2.82$, $p = 0.011$, $d = 0.82$), and medulla ($t [45] = -2.44$, $p = 0.019$, $d = 0.71$) (Fig. 2B, Table 2).

Similar results were found, when excluding the data sets of the three late-onset patients ($N = 21$). Additionally, typical-onset patients showed significantly increased TSC values in cerebellar WM compared to controls ($t [42] = -2.20$, $p = 0.045$; $d = 0.64$) (Supplementary Table 1).

3.3. Correlation analysis

In controls, there were significant negative correlations between age and brain volume in several cerebral lobes, with effect sizes ranging from $r = -0.50$ in the left frontal lobe to $r = -0.57$ in the left parietal lobe. Higher TSC was significantly related to older age in nearly all cerebral lobes ranging from $r = 0.43$ in right occipital lobe to $r = 0.68$ in right frontal lobe, in the cerebellum ranging from $r = 0.47$ in total cerebellum to $r = 0.53$ in right cerebellar lobules I-V and left lobules VI-VII, and in the brainstem (midbrain; $r = 0.50$) (Supplementary Table 2).
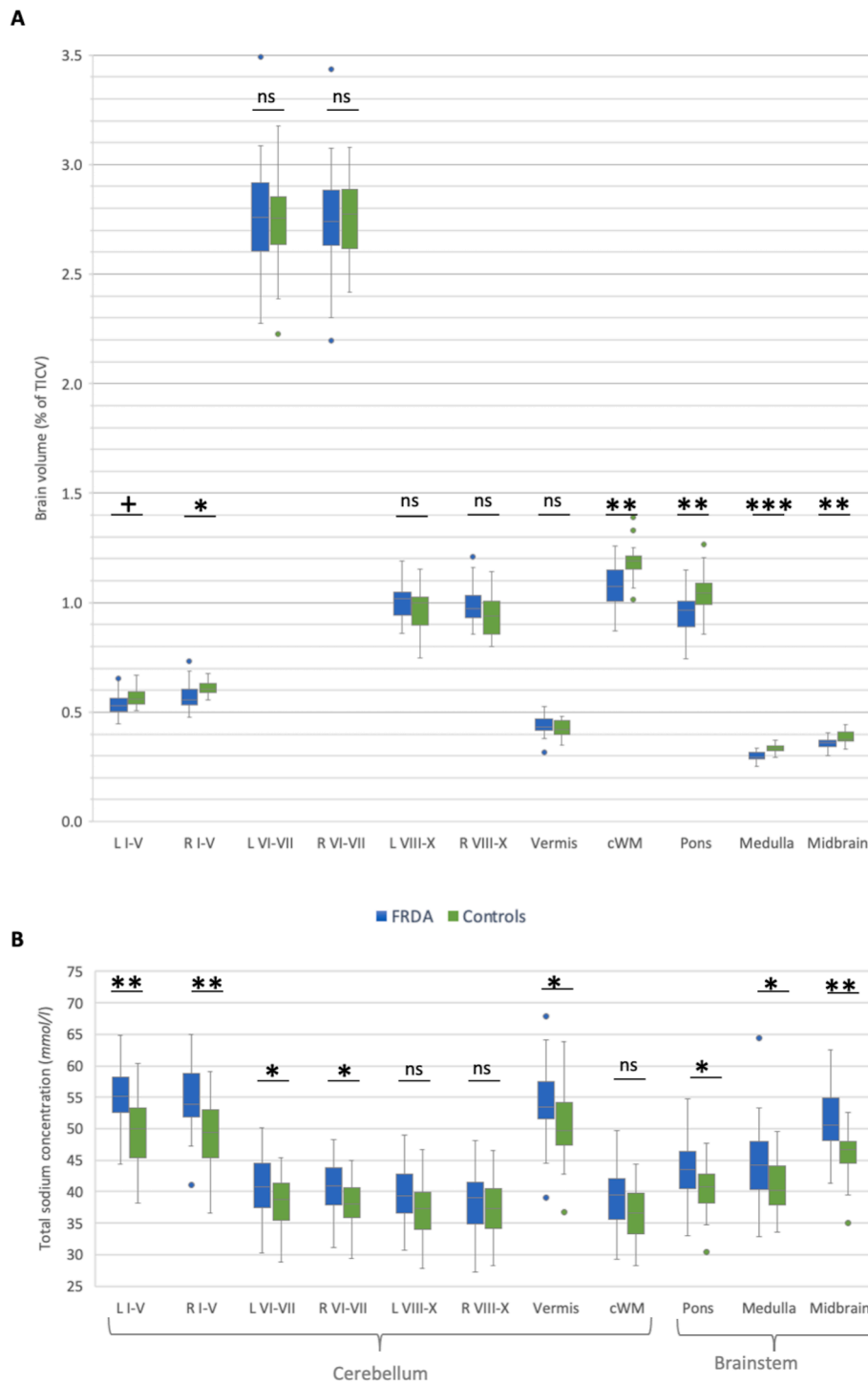
In patients with Friedreich ataxia, there were significant correlations in the cerebral lobes between older age and lower volume in right frontal lobe ($r = -0.48$), left ($r = -0.45$) and right parietal lobe ($r = -0.65$), and higher TSC values in right parietal lobe ($r = 0.44$) (Supplementary Table 2). After controlling for age, lower brain volume in left cerebellar lobules I-V was significantly related to higher GAA repeat numbers on allele 1 ($r = -0.43$), and in cerebellar WM to higher disability stages ($r = -0.62$), SARA scores ($r = -0.56$), and ADL ratings ($r = -0.52$; Fig. 3A). Increased TSC values in the right cerebellar lobules I-V were significantly correlated with younger age at onset ($r = -0.43$) and accordingly longer disease duration ($r = 0.43$; Fig. 3B). Other correlations between TSC and brain volume or clinical variables did not reach significance (e. g. negative correlation between TSC and brain volume in the left parietal lobe [$r = -0.40$, $p = 0.058$]; positive correlation between TSC in the right cerebellar lobules I-V and SARA scores [$r = 0.40$, $p = 0.061$]; see Supplementary Table 2).

4. Discussion

Our study provides first insights into metabolic sodium changes in individuals with Friedreich ataxia. Infra-tentorial TSC levels were increased in patients with Friedreich ataxia compared to controls, whereas volumes in brainstem and cerebellum were decreased in the patient group, in line with established findings (Dogan et al., 2016; Dogan et al., 2018) Hence, both metabolic and structural changes were exclusively revealed in the hallmark structures in Friedreich ataxia. However, sodium MRI showed additional changes, particularly in cerebellar subregions where structural differences could not be detected. Structural MRI on the other hand showed more associations with clinical parameters.

Increased TSC levels were evident in the brainstem, including pons, medulla, and midbrain. However, beyond the structural changes, we found an increase of TSC levels in other cerebellar subregions, namely in left (and right) cerebellar lobules I-V, VI-VII, and vermis. Excluding patients with late disease onset and comparing only Friedreich ataxia patients with typical onset with controls, metabolic changes in cerebellar WM were also evident. Since earlier age of disease onset is

Fig. 2. Group comparisons in brain volume and total sodium concentration in cerebellar and brainstem subregions between patients with Friedreich ataxia ($N = 24$) versus controls ($N = 23$). (A) Group differences in brain volumes. (B) Group differences in total sodium concentration. Data of brain volumes are adjusted for total intracranial volume (TICV) and displayed as percentage; $*p < 0.05$, $**p < 0.01$ or $***p < 0.001$ (significance thresholds); + not significant after Benjamini-Hochberg procedure (p greater than 0.05). *Abbreviations*: FRDA = Friedreich ataxia; L = left hemisphere; R = right hemisphere; I-X = cerebellar lobules I-X; cWM = cerebellar white matter.

associated with a more severe disease course, sodium changes as an indicator of cellular dysfunction in cerebellar WM may be related to such a more pronounced course of disease. Additionally, elevated TSC values in right cerebellar lobules IV were associated to patients' younger age at onset and longer disease duration in patients. The ability of sodium MRI to detect such a biological link to disease-specific parameters in combination with the indication of metabolic dysfunction offers a promising starting point for potential monitoring of disease progression over time.

Simultaneously, reduced brain volume was shown in the right cerebellar lobules I-V and cerebellar WM, and in the brainstem, including pons, medulla, and midbrain. Our results generally accord

with findings in a recent project by the ENIGMA-Ataxia Working Group (Harding et al., 2021), in which data of 248 patients with Friedreich ataxia from ten study sites (including Aachen) were retrospectively examined, showing strongest volumetric differences in the brainstem, dentate nucleus region, superior and inferior cerebellar peduncles, and anterior cerebellar gray matter lobules I–VI. However, the authors also reported cerebral differences, particularly in precentral gyri and corticospinal tracts, likely manifesting during the course of the disease (Harding et al., 2021). Although most of patients were in an intermediate or late disease stage, the lack of cerebral volumetric group differences in our analysis is most probably related to the reduced power of the small sample size in the current project, similar to other volumetric
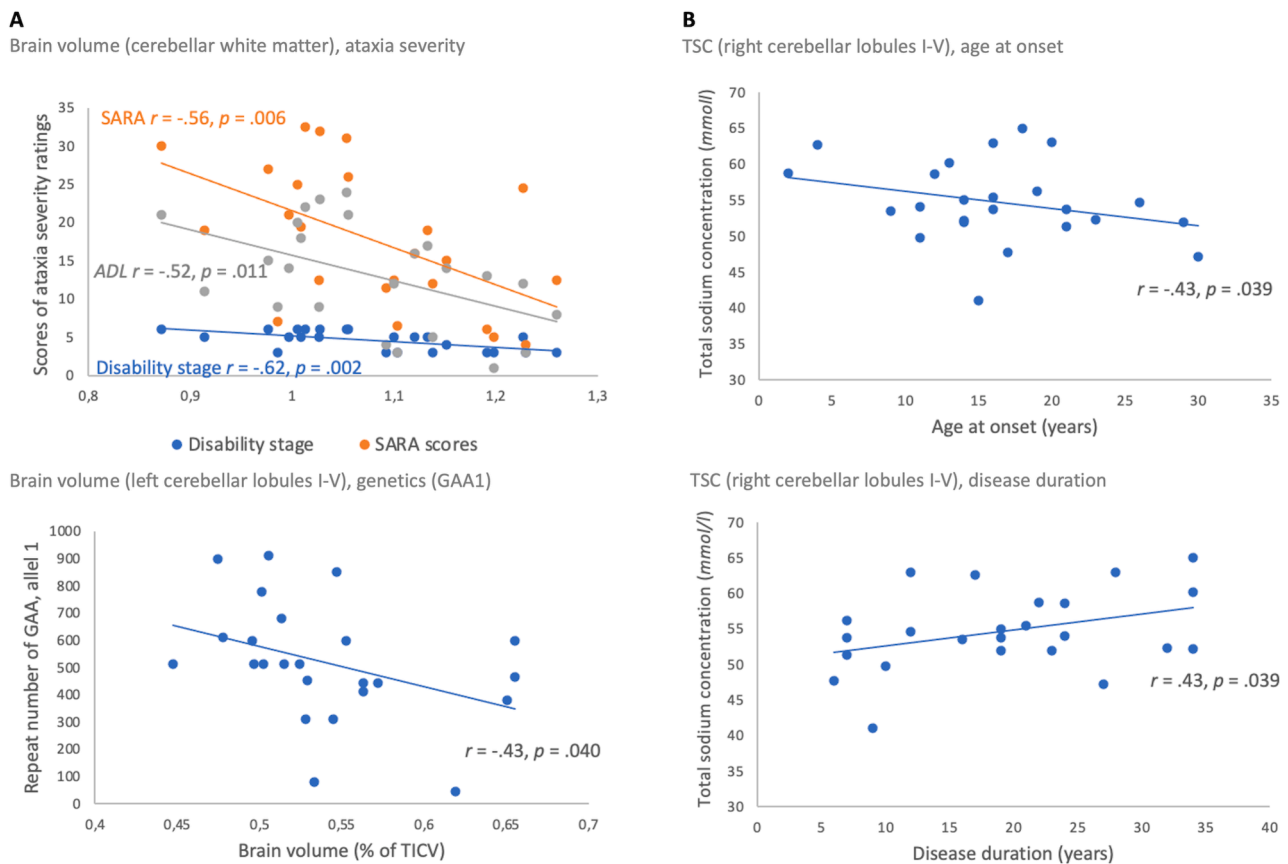
Fig. 3. Correlations of MRI data with clinical variables in patients with Friedreich ataxia ($p < 0.05$). (A) Correlations with brain volume data. **(B)** Correlations with total tissue sodium concentration (TSC). *Abbreviations:* SARA = scale for the assessment and rating of ataxia; ADL = activity of daily living scale; TICV = total intracranial volume.

studies in Friedreich ataxia (Dogan et al., 2018; Nave et al., 2008), in contrast to the large-scale ENIGMA-project allowing more sensitive and stage-dependent volumetric analyses. Correlation analysis between clinical parameters and brain volume data revealed that reduced brain volume in left cerebellar lobules I-V was inversely associated to genetic parameters, namely increased GAA repeat numbers on allele 1, and in cerebellar WM to more severe ataxia, represented by higher disability stages, increased SARA scores, and increased ADL ratings. These results are in accordance with previous findings on structural MRI and severity of ataxia (Dogan et al., 2018; Akhlaghi et al., 2011; Pagani et al., 2010; Selvadurai et al., 2016).

In cerebellar hemispheres and vermis, increases in TSC levels were present in Friedreich ataxia patients without concomitant significant atrophy in corresponding regions. Despite correction for partial volume effects, cerebellar cortex regions may be more prone to sodium signals originating from neighboring CSF. On the other hand, given that cerebellar gray matter loss usually occurs later in the course of the disease, (Harding et al., 2021) this might also support the potential of sodium MR to provide additional information at a basic biochemical level where increases of intracellular sodium concentration may precede neurodegenerative volume loss. In Friedreich ataxia, mitochondrial ATP production is deficient (Lodi et al., 1999); this results in energy failure of the Na^+/K^+-ATPase ion pumps, as the Na^+/K^+-ATPase is highly dependent on energy in form of ATP. However, this resting potential is essential for cell homeostasis and sufficient neurotransmission. Consequently, this imbalance causes loss of the ion homeostasis across cell membranes. The change in distribution of ion concentrations between tissue compartments is the harbinger of deficient neurotransmission, cell dysfunction and death, (Thulborn, 2018) measured by increased TSC levels – as a quantitative bioscale of the cellular metabolism. In Friedreich ataxia,

most energy is probably utilized in the synapses rather than in the cell body to repolarize the cells and activate ion pumps as well as ion exchangers. This impaired cellular metabolism and potentially disturbed interneuronal communication due to energy-dependent altered homeostasis might offer an explanation for sodium changes without concomitant atrophy, particularly in the cerebellar cortex. This could help to identify disease-specific areas affected at probably early disease stages and potentially inform about degenerative processes.

These current findings on infratentorial TSC levels in Friedreich ataxia give first indications on the potential of sodium MRI to monitor metabolic changes, and future longitudinal studies will be essential to assess the utility of sodium MRI to potentially track early processes of neurodegeneration. Early detection of neurodegenerative diseases is of particular interest in order to be able to intervene at an early stage in the course of the disease or monitor potential treatment effects in the future. Especially in light of upcoming clinical trials, it is crucial to identify valid and sensitive biomarkers to improve clinical trial design and verify treatment efficacy as early as possible. In particular for diseases with long preclinical phases, or a slowly progressive nature such as Friedreich ataxia, prevention or early interventions are of upmost importance. Using sodium MRI, the current findings show that TSC appears to be sensitive to quantify metabolic changes in Friedreich ataxia and needs to be evaluated in further research and longitudinal assessments.

The sodium imaging technique used in the current study measures TSC by assessing the volume-fraction-weighted mean of the intracellular sodium concentration and the extracellular sodium concentration (Christensen et al., 1996). Differentiation into intra- and extracellular sodium concentrations would be highly desirable and would allow a more accurate assessment of biochemical changes, which is currently methodologically difficult. There are some attempts to estimate the

relative proportions between intra- and extracellular sodium, such as using shift reagents in animal models (Winter and Bansal, 2001). Another qualitative method to differentiate the sodium signal is relaxation-weighted sodium MRI, as demonstrated by Nagel et al., (Nagel et al., 2011) on patients with brain tumors, although this relaxation-weighted sodium signal is not necessarily congruent with intra- or extracellular space (Nagel et al., 2011).

4.1. Limitations and outlook

Regarding technical issues and feasibility, sodium MR imaging can potentially be well integrated into a clinical setting; in particular from a time perspective as the total scan time is about 18 min. In addition, these initial results were acquired with a 3 Tesla scanner, which is frequently used in clinical practice. The advantage here is the good availability. Although additional MRI components such as the ^{1}H/^{23}Na quadrature birdcage coil and phantoms are needed, it would be desirable to further intensify its application and foster more routine usage also in other research centers. However, higher-field scanners of more than 3 Tesla with improved SNR could help to overcome the problem of lower SNR ratios in sodium imaging in future application (Mellon et al., 2009; Haeger et al., 2021). Regarding the two-point calibration curve to transform ^{23}Na M_0 images into TSC maps one could argue that a higher number of agarose references might be more accurate. However, previous work has successfully used a calibration with two points, (Inglese et al., 2010; Reetz et al., 2012; Coste et al., 2019) and there are other attempts where even one reference is used such as implementing the calibration with the knowledge of sodium concentrations in CSF (Qian et al., 2012). Therefore, to achieve our goal of making sodium measurement clinically practical, we used the time-efficient two-point calibration instead of multiple references. With a resolution of 4 mm isotropic of the sodium images, it was demanding to distinguish between WM and GM (gray matter) in the cerebellum with its fine ramifications. Another issue concerns the cerebrospinal fluid (CSF), as it is difficult to distinguish the sodium signal coming from brain tissue and nearby CSF, (Thulborn et al., 2016) particularly in the cortical regions of the cerebellum. Thus, due to the low resolution of the sodium images it cannot be entirely ruled out that the TSC levels of the cerebellar regions investigated in this study, although being corrected for partial volume effects, may still include sodium signals originating from neighboring CSF. This may be reflected by the positive association between increased age and higher TSC values in the control group, as Thulborn *et al.,* (Thulborn et al., 2016) argued that the TSC remains stable in the human brain during normal aging, whereas the space occupied by the CSF is increasing with age due to tissue loss during aging. Although no such correlations of age and TSC were detected in the cerebellum or brainstem of the patients in the current study, we included age as a covariate in the partial correlation analysis and explicitly matched both groups for age and sex to avoid potential confounding age effects. With a mean disease duration of 19.3 ± 9.2 years, our investigated Friedreich ataxia cohort formed a quite affected patient sample with SARA ratings on average of 17.8 ± 9.1 points. This may be one of the reasons why differences in brain volume and TSC were largely overlapping. Due to the recessive inheritance of the disease and usually early onset in childhood, it is challenging to include mildly affected participants. In other neurodegenerative disease, such as Huntington's disease, where preclinical genetic testing is possible due to autosomal dominant inheritance, metabolic imaging can offer new insights into prodromal neuropathological stages (Reetz et al., 2012).

Currently, the resolution of 4 mm isotropic of the sodium images is too low to investigate metabolic changes in the spinal cord. Since spinal cord and dorsal spinal ganglia are the primarily affected structures in Friedreich ataxia, it will be important for future developments to assess TSC in these key regions (Koeppen and Mazurkiewicz, 2013). Likewise, with regard to cerebellar segmentation approaches, the dentate nuclei as an important target in the disease should be considered in future segmentation approaches for TSC measurements. In Friedreich ataxia, it would be desirable to include young children and adolescents in future

research to investigate sodium MRI as an early imaging marker. In particular, longitudinal studies with larger sample sizes allowing stage-dependent subgroup analysis and assessments of metabolic changes over time could provide critical insights on the sensitivity of sodium compared to structural MRI.

5. Conclusions

Our findings suggest the potential of *in vivo* sodium MRI to detect quantitative metabolic changes of total tissue sodium concentration in the key regions in Friedreich ataxia, the cerebellum and brainstem. There were no supratentorial sodium increases in our patients compared to healthy controls. The complementary contribution of sodium MRI to monitor early degenerative processes is further supported by TSC increases in several cerebellar regions without concomitant atrophy in these regions, indicating that sodium MRI as a new bioscale may shed additional insights into metabolic pathophysiological mechanisms of Friedreich ataxia. Associations of increased TSC levels with younger age at disease onset or longer disease duration additionally support sodium MRI as an indicator of disease progression. However, longitudinal studies are necessary to assess TSC changes over time and to further elucidate the reliability and sensitivity of sodium MRI to detect early metabolic changes and monitor disease progression in Friedreich ataxia.

CRediT authorship contribution statement

Janna Krahe: Data curation, Formal analysis, Investigation, Methodology, Software, Validation, Visualization, Writing – original draft. **Imis Dogan:** Investigation, Methodology, Validation, Writing – review & editing. **Claire Didszun:** Investigation, Writing – review & editing. **Shahram Mirzazade:** Investigation, Writing – review & editing. **Alexa Haeger:** Writing – review & editing. **Nadim Joni Shah:** Writing – review & editing. **Ilaria A. Giordano:** Writing – review & editing. **Thomas Klockgether:** Writing – review & editing. **Guillaume Madelin:** Writing – review & editing. **Jörg B. Schulz:** Resources, Writing – review & editing. **Sandro Romanzetti:** Conceptualization, Data curation, Formal analysis, Investigation, Methodology, Project administration, Software, Supervision, Validation, Visualization, Writing – review & editing. **Kathrin Reetz:** Conceptualization, Formal analysis, Funding acquisition, Methodology, Project administration, Resources, Supervision, Validation, Writing – review & editing.

Declaration of Competing Interest

The authors declare that they have no known competing financial interests or personal relationships that could have appeared to influence the work reported in this paper.

269953372/GRK2150), and by the Brain Imaging Facility, a Facility of the Interdisciplinary Centre for Clinical Research (IZKF) Aachen within the Faculty of Medicine at RWTH Aachen University. All anatomical registrations were performed with computing resources granted by RWTH Aachen University under project rwth0212.

Appendix A. Supplementary data

Supplementary data to this article can be found online at https://doi.org/10.1016/j.nicl.2022.103025.

References

Campuzano, V., Montermini, L., Moltò, M.D., et al., 1996. Friedreich's ataxia: autosomal recessive disease caused by an intronic GAA triplet repeat expansion. Science 271 (5254), 1423–1427. https://doi.org/10.1126/science.271.5254.1423.

Harding, A.E., 1981. Friedreich's ataxia: A clinical and genetic study of 90 families with an analysis of early diagnostic criteria and intrafamilial clustering of clinical features. Brain. 104 (3), 589–620. https://doi.org/10.1093/brain/104.3.589.

Hewer, R.L., 1968. Study of fatal cases of Friedreich's Ataxia. Brit med J. 3 (September), 649–652.

Thorén, C., 1962. Diabetes mellitus in Friedreich's ataxia. Acta Paediatr. 51 (s135), 239–247.

Reetz, K., Dogan, I., Hohenfeld, C., Didszun, C., Giunti, P., Mariotti, C., Durr, A., Boesch, S., Klopstock, T., Rodríguez de Rivera Garrido, F.J., Schöls, L., Giordano, I., Bürk, K., Pandolfo, M., Schulz, J.B., 2018. Nonataxia symptoms in Friedreich Ataxia: report from the registry of the European Friedreich's Ataxia consortium for translational studies (EFACTS). Neurology. 91 (10), e917–e930.

Friedreich, N., 1863. Ueber degenerative Atrophie der spinalen Hinterstränge. Arch. Pathol. Anat. Physiol. Klin. Med. 26 (3-4), 391–419.

Reetz, K., Dogan, I., Costa, A.S., Dafotakis, M., Fedosov, K., Giunti, P., Parkinson, M.H., Sweeney, M.G., Mariotti, C., Panzeri, M., Nanetti, L., Arpa, J., Sanz-Gallego, I., Durr, A., Charles, P., Boesch, S., Nachbauer, W., Klopstock, T., Karin, I., Depondt, C., vom Hagen, J.M., Schöls, L., Giordano, I.A., Klockgether, T., Bürk, K., Pandolfo, M., Schulz, J.B., 2015. Biological and clinical characteristics of the European Friedreich's Ataxia Consortium for Translational Studies (EFACTS) cohort: A cross-sectional analysis of baseline data. Lancet Neurol. 14 (2), 174–182.

Reetz, K., Dogan, I., Hilgers, R.-D., Giunti, P., Mariotti, C., Durr, A., Boesch, S., Klopstock, T., de Rivera, F.J.R., Schöls, L., Klockgether, T., Bürk, K., Rai, M., Pandolfo, M., Schulz, J.B., Nachbauer, W., Eigentler, A., Depondt, C., Benaich, S., Charles, P., Ewenczyk, C., Monin, M.-L., Dafotakis, M., Fedosov, K., Didszun, C., Ermis, U., Giordano, I.A., Timmann, D., Karin, I., Neuhofer, C., Stendel, C., Müller vom Hagen, J., Wolf, J., Panzeri, M., Nanetti, L., Castaldo, A., Arpa, J., Sanz-Gallego, I., Parkinson, M.H., Sweeney, M.G., 2016. Progression characteristics of the European Friedreich's Ataxia Consortium for Translational Studies (EFACTS): a 2 year cohort study. Lancet Neurol. 15 (13), 1346–1354.

Reetz, K., Dogan, I., Hilgers, R.-D., Giunti, P., Parkinson, M.H., Mariotti, C., Nanetti, L., Durr, A., Ewenczyk, C., Boesch, S., Nachbauer, W., Klopstock, T., Stendel, C., Rodríguez de Rivera Garrido, F.J., Rummey, C., Schöls, L., Hayer, S.N., Klockgether, T., Giordano, I., Didszun, C., Rai, M., Pandolfo, M., Schulz, J.B., Labrum, R., Thomas-Black, G., Manso, K., Solanky, N., Gellera, C., Mongelli, A., Castaldo, A., Fichera, M., Palau, F., O'Callaghan, M., Biet, M., Monin, M.L., Eigentler, A., Indelicato, E., Amprosi, M., Radelfahr, F., Bischoff, A.T., Holtbernd, F., Brcina, N., Hohenfeld, C., Koutsis, G., Breza, M., Bertini, E., Vasco, G., 2021. Progression characteristics of the European Friedreich's Ataxia Consortium for Translational Studies (EFACTS): a 4-year cohort study. Lancet Neurol. 20 (5), 362–372.

Metz G., Coppard N., Cooper J.M., et al., Rating disease progression of Friedreich's ataxia by the International Cooperative Ataxia Rating Scale: Analysis of a 603-patient database, Brain, 2013;136(1):259-268, 10.1093/brain/aws309.

França, M.C., D'Abreu, A., Yasuda, C.L., Bonadia, L.C., Santos da Silva, M., Nucci, A., Lopes-Cendes, I., Cendes, F., 2009. A combined voxel-based morphometry and 1H-MRS study in patients with Friedreich's ataxia. J. Neurol. 256 (7), 1114–1120.

Dogan, I., Tinnemann, E., Romanzetti, S., Mirzazade, S., Costa, A.S., Werner, C.J., Heim, S., Fedosov, K., Schulz, S., Timmann, D., Giordano, I.A., Klockgether, T., Schulz, J.B., Reetz, K., 2016. Cognition in Friedreich's ataxia: a behavioral and multimodal imaging study. Ann. Clin. Transl. Neurol. 3 (8), 572–587.

Dogan, I., Romanzetti, S., Didszun, C., et al., 2018. Structural characteristics of the central nervous system in Friedreich ataxia: An in vivo spinal cord and brain MRI study. J. Neurol. Neurosurg. Psychiatry 1–3. https://doi.org/10.1136/jnnp-2018-318422.

Koeppen, A.H., Mazurkiewicz, J.E., 2013. Friedreich Ataxia : neuropathology revised. J. Neuropathol. Exp. Neurol. 72 (2), 78–90.

Reetz, K., Hilgers, R.-D., Isfort, S., Dohmen, M., Didszun, C., Fedosov, K., Kistermann, J., Mariotti, C., Durr, A., Boesch, S., Klopstock, T., Rodríguez de Rivera Garrido, F.J., Schöls, L., Klockgether, T., Pandolfo, M., Korinthenberg, R., Lavin, P., Molenberghs, G., Libri, V., Giunti, P., Festenstein, R., Schulz, J.B., 2019. Protocol of a randomized, double-blind, placebo-controlled, parallel-group, multicentre study of the efficacy and safety of nicotinamide in patients with Friedreich ataxia (NICOFA). Neurol Res Pract. 1 (1) https://doi.org/10.1186/s42466-019-0038-9.

Madelin, G., Regatte, R.R., 2013. Biomedical applications of sodium MRI in vivo. J. Magn. Reson. Imaging 38, 511–529. https://doi.org/10.1002/jmri.24168.

Boada, F.E., LaVerde, G., Jungreis, C., Nemoto, E., Tanase, C., Hancu, I., 2005. Loss of cell ion homeostasis and cell viability in the brain: what sodium MRI can tell us. Curr. Top. Dev. Biol. 70, 77–101. https://doi.org/10.1016/S0070-2153(05)70004-1.

Christensen, J.D., Barrère, B.J., Boada, F.E., Vevea, J.M., Thulborn, K.R., 1996. Quantitative tissue sodium concentration mapping of normal rat brain. Magn. Reson. Med. 36 (1), 83–89. https://doi.org/10.1002/mrm.1910360115.

Hashimoto, T., Ikehira, H., Fukuda, H., et al., 1991. In vivo sodium-23 MRI in brain tumors: evaluation of preliminary clinical experience. Am J Physiol Imaging. 6 (2), 74–80.

Ouwerkerk R., Bleich K.B., Gillen J.S., Pomper M.G., Radiology in human brain tumors as measured with 23 Na MR, 2003;23(10):529-537.

Thulborn, K.R., Lu, A., Atkinson, I.C., Damen, F., Villano, J.L., 2009. Quantitative sodium MR Imaging and sodium bioscales for the management of brain tumors. Neuroimaging Clin. N. Am. 19 (4), 615–624. https://doi.org/10.1016/j.nic.2009.09.001.

Nagel, A.M., Bock, M., Hartmann, C., Gerigk, L., Neumann, J.-O., Weber, M.-A., Bendszus, M., Radbruch, A., Wick, W., Schlemmer, H.-P., Semmler, W., Biller, A., 2011. The potential of relaxation-weighted sodium magnetic resonance imaging as demonstrated on brain tumors. Invest. Radiol. 46 (9), 539–547.

Thulborn, K.R., Gindin, T.S., Davis, D., Erb, P., 1999. Comprehensive MR imaging protocol for stroke management: tissue sodium concentration as a measure of tissue viability in nonhuman primate studies and in clinical studies. Radiology 213 (1), 156–166.

Hussain, M.S., Stobbe, R.W., Bhagat, Y.A., Emery, D., Butcher, K.S., Manawadu, D., Rizvi, N., Maheshwari, P., Scozzafava, J., Shuaib, A., Beaulieu, C., 2009. Sodium imaging intensity increases with time after human ischemic stroke. Ann. Neurol. 66 (1), 55–62.

Inglese, M., Madelin, G., Oesingmann, N., et al., 2010. Brain tissue sodium concentration in multiple sclerosis : a sodium imaging study at 3 tesla. Brain. 133 (3), 847–857. https://doi.org/10.1093/brain/awp334.

Boada, F.E., Qian, Y., Nemoto, E., Jovin, T., Jungreis, C., Jones, S.C., Weimer, J., Lee, V., 2012. Sodium MRI and the assessment of irreversible tissue damage during hyper-acute stroke. Transl Stroke Res. 3 (2), 236–245.

Zaaraoui, W., Konstandin, S., Audoin, B., et al., 2012. Distribution of brain sodium accumulation correlates with disability in multiple sclerosis. Radiology 264 (3), 859–867. https://doi.org/10.1148/radiol.12112680/-/DC1.

Petracca, M., Vancea, R.O., Fleysher, L., Jonkman, L.E., Oesingmann, N., Inglese, M., 2016. Brain intra- and extracellular sodium concentration in multiple sclerosis: A 7 T MRI study. Brain. 139 (3), 795–806. https://doi.org/10.1093/brain/awv386.

Mellon, E.A., Pilkinton, D.T., Clark, C.M., Elliott, M.A., Witschey, W.R., Borthakur, A., Reddy, R., 2009. Sodium MR imaging detection of mild Alzheimer disease: preliminary study. Am. J. Neuroradiol. 30 (5), 978–984.

Reetz, K., Romanzetti, S., Dogan, I., Saß, C., Werner, C.J., Schiefer, J., Schulz, J.B., Shah, N.J., 2012. Increased brain tissue sodium concentration in Huntington's Disease — A sodium imaging study at 4 T. Neuroimage. 63 (1), 517–524.

Haeger, A., Bottlaender, M., Lagarde, J., Porciuncula Baptista, R., Rabrait-Lerman, C., Luecken, V., Schulz, J.B., Vignaud, A., Sarazin, M., Reetz, K., Romanzetti, S., Boumezbeur, F., 2021. What can 7T sodium MRI tell us about cellular energy depletion and neurotransmission in Alzheimer's Disease? Alzheimer's Dement. 17 (11), 1843–1854.

Haeger, A., Costa, A.S., Romanzetti, S., Kilders, A., Trautwein, C., Haberl, L., Beulertz, M., Hildebrand, F., Schulz, J.B., Reetz, K., 2020. Effect of a multicomponent exercise intervention on brain metabolism: A randomized controlled trial on Alzheimer's pathology (Dementia-MOVE). Alzheimer's Dement Transl Res Clin Interv. 6 (1) https://doi.org/10.1002/trc2.12032.

Vorgerd, M., Schöls, L., Hardt, C., Ristow, M., Epplen, J.T., Zange, J., 2000. Mitochondrial impairment of human muscle in Friedreich ataxia in vivo. Neuromuscul. Disord. 10 (6), 430–435. https://doi.org/10.1016/S0960-8966(00)00108-5.

Hart, P.E., Lodi, R., Rajagopalan, B., Bradley, J.L., Crilley, J.G., Turner, C., Blamire, A.M., Manners, D., Styles, P., Schapira, A.H.V., Cooper, J.M., 2005. Antioxidant treatment of patients with Friedreich Ataxia. Arch. Neurol. 62 (4), 621.

Lodi, R., Cooper, J.M., Bradley, J.L., Manners, D., Styles, P., Taylor, D.J., Schapira, A.H. V., 1999. Deficit of in vivo mitochondrial ATP production in patients with Friedreich ataxia. Proc Natl Acad Sci U S A. 96 (20), 11492–11495.

Schmitz-Hubsch, T., du Montcel, S.T., Baliko, L., Berciano, J., Boesch, S., Depondt, C., Giunti, P., Globas, C., Infante, J., Kang, J.-S., Kremer, B., Mariotti, C., Melegh, B., Pandolfo, M., Rakowicz, M., Ribai, P., Rola, R., Schols, L., Szymanski, S., van de Warrenburg, B.P., Durr, A., Klockgether, T., 2006. Scale for the assessment and rating of ataxia: development of a new clinical scale. Neurology. 66 (11), 1717–1720.

Subramony, S.H., May, W., Lynch, D., Gomez, C., Fischbeck, K., Hallett, M., Taylor, P., Wilson, R., Ashizawa, T., 2005. Measuring Friedreich ataxia: Interrater reliability of a neurologic rating scale. Neurology. 64 (7), 1261–1262.

Anheim M., Monga B., Fleury M., et al. Ataxia with oculomotor apraxia type 2: clinical, biological and genotype/phenotype correlation study of a cohort of 90 patients, Brain, 2009;132(10):2688-2698, 10.1093/brain/awp214.

Coste, A., Boumezbeur, F., Vignaud, A., et al., 2019. Tissue sodium concentration and sodium T 1 mapping of the human brain at 3 T using a Variable Flip Angle method. Magn. Reson. Imaging 58, 116–124. https://doi.org/10.1016/j.mri.2019.01.015.

Pipe, J.G., Zwart, N.R., Aboussouan, E.A., Robison, R.K., Devaraj, A., Johnson, K.O., 2011. A new design and rationale for 3D orthogonal oversampled k-space trajectories. Magn. Reson. Med. 66 (5), 1303–1311. https://doi.org/10.1002/mrm.22918.

Tustison, N.J., Cook, P.A., Klein, A., Song, G., Das, S.R., Duda, J.T., Kandel, B.M., van Strien, N., Stone, J.R., Gee, J.C., Avants, B.B., 2014. Large-scale evaluation of ANTs and FreeSurfer cortical thickness measurements. Neuroimage. 99, 166–179.

Avants, B.B., Tustison, N.J., Song, G., Cook, P.A., Klein, A., Gee, J.C., 2011. A reproducible evaluation of ANTs similarity metric performance in brain image registration. Neuroimage. 54 (3), 2033–2044. https://doi.org/10.1016/j.neuroimage.2010.09.025.

Diedrichsen, J., 2006. A spatially unbiased atlas template of the human cerebellum. Neuroimage. 33 (1), 127–138. https://doi.org/10.1016/j.neuroimage.2006.05.056.

Wang, H., Suh, J.W., Das, S.R., Pluta, J.B., Craige, C., Yushkevich, P.A., 2013. Multi-atlas segmentation with joint label fusion. IEEE Trans. Pattern Anal. Mach. Intell. 35 (3), 611–623. https://doi.org/10.1109/TPAMI.2012.143.

Hua, X., Leow, A.D., Parikshak, N., Lee, S., Chiang, M.-C., Toga, A.W., Jack, C.R., Weiner, M.W., Thompson, P.M., 2008. Tensor-based morphometry as a neuroimaging biomarker for Alzheimer's disease: An MRI study of 676 AD, MCI, and normal subjects. Neuroimage. 43 (3), 458–469.

Fessler, J.A., Sutton, B.P., 2003. Nonuniform fast Fourier transforms using min-max interpolation. IEEE Trans. Signal Process. 51 (2), 560–574. https://doi.org/10.1109/TSP.2002.807005.

Thomas, B.A., Cuplov, V., Bousse, A., Mendes, A., Thielemans, K., Hutton, B.F., Erlandsson, K., 2016. PETPVC: A toolbox for performing partial volume correction techniques in positron emission tomography. Phys. Med. Biol. 61 (22), 7975–7993.

Cohen, J., 1988. Statistical power analysis for the behavioral sciences, 2nd ed. Academic press, New York.

Benjamini, Y., Hochberg, Y., 1995. Controlling the false discovery rate: a practical and powerful approach to multiple testing. J. R. Stat. Soc. Ser. B. 57 (1), 289–300. http://links.jstor.org/sici?sici=0035-9246%281995%2957%3A1%3C289%3ACTFDRA%3E2.0.CO%3B2-E.

Harding, I.H., Chopra, S., Arrigoni, F., et al., 2021. Brain structure and degeneration staging in friedreich ataxia: magnetic resonance imaging volumetrics from the ENIGMA-ataxia working group. Ann. Neurol. 90 (4), 570–583. https://doi.org/10.1002/ana.26200.

Nave, R.D., Ginestroni, A., Giannelli, M., Tessa, C., Salvatore, E., Salvi, F., Dotti, M.T., De Michele, G., Piacentini, S., Mascalchi, M., 2008. Brain structural damage in Friedreich ' s ataxia. J. Neurol. Neurosurg. Psychiatry 79 (1), 82–85.

Akhlaghi, H., Corben, L., Georgiou-Karistianis, N., Bradshaw, J., Storey, E., Delatycki, M. B., Egan, G.F., 2011. Superior cerebellar peduncle atrophy in Friedreich's ataxia correlates with disease symptoms. Cerebellum. 10 (1), 81–87.

Pagani, E., Ginestroni, A., Della Nave, R., Agosta, F., Salvi, F., De Michele, G., Piacentini, S., Filippi, M., Mascalchi, M., 2010. Assessment of brain white matter fiber bundle atrophy in patients with Friedreich ataxia. Radiology 255 (3), 882–889.

Selvadurai, L.P., Harding, I.H., Corben, L.A., Stagnitti, M.R., Storey, E., Egan, G.F., Delatycki, M.B., Georgiou-Karistianis, N., 2016. Cerebral and cerebellar grey matter atrophy in Friedreich ataxia: the IMAGE-FRDA study. J. Neurol. 263 (11), 2215–2223.

Thulborn, K.R., 2018. Quantitative sodium MR imaging: a review of its evolving role in medicine. Neuroimage. 168, 250–268. https://doi.org/10.1016/j.neuroimage.2016.11.056.

Winter, P.M., Bansal, N., 2001. TmDOTP5- as a 23Na shift reagent for the subcutaneously implanted 9L gliosarcoma in rats. Magn. Reson. Med. 45 (3), 436–442. https://doi.org/10.1002/1522-2594(200103)45:3<436::AID-MRM1057>3.0.CO;2-6.

Qian, Y., Zhao, T., Zheng, H., Weimer, J., Boada, F.E., 2012. High-resolution sodium imaging of human brain at 7 T. Magn. Reson. Med. 68 (1), 227–233. https://doi.org/10.1002/mrm.23225.

Thulborn, K.R., Lui, E., Guntin, J., et al., 2016. Quantitative sodium MR imaging of the human brain at 9.4 tesla provides assessment of tissue sodium concentration and cell volume fraction during normal ageing. NMR Biomed. 29 (2), 137–143. https://doi.org/10.1002/nbm.3312.